Anal. Chem. **2003,** *75,* 1180−1187

On-Chip Coupling of Isoelectric Focusing and Free Solution Electrophoresis for Multidimensional Separations

Amy E. Herr,*[,†,‡] Joshua I. Molho,[†,§] Katerina A. Drouvalakis,[∥] James C. Mikkelsen,[§,⊥] Paul J. Utz,[∥] Juan G. Santiago,[†] and Thomas W. Kenny[†]

Department of Mechanical Engineering, Department of Chemical Engineering, and Department of Medicine, Stanford University, Stanford, California 94305-4021

We have developed an acrylic microfluidic device that sequentially couples liquid-phase isoelectric focusing (IEF) and free solution capillary electrophoresis (CE). Rapid separation (<1 min) and preconcentration (73×) of species were achieved in the initial IEF dimension. Using full-field fluorescence imaging, we observed non-dispersive mobilization velocities on the order of 20 μm/s during characterization of the IEF step. This transport behavior allowed controlled electrokinetic mobilization of focused sample bands to a channel junction, where voltage switching was used to repeatedly inject effluent from the IEF dimension into an ampholyte-based CE separation. This second dimension was capable of analyzing all fluid volumes of interest from the IEF dimension, as IEF was 'parked' during each CE analysis and refocused prior to additional CE analyses. Investigation of each dimension of the integrated system showed time-dependent species displacement and band-broadening behavior consistent with IEF and CE, respectively. The peak capacity of the 2D system was ∼1300. A comprehensive 2D analysis of a fluid volume spanning 15% of the total IEF channel length was completed in less than 5 min.

Multidimensional separations aid in accurate identification and quantification of specific proteins present in complex samples.[1−3] In a two-dimensional (2D) separation, two independent separation mechanisms are employed sequentially, each providing a selective displacement along respective separation axes.[4] Conventional implementations of 2D systems include slab-gel and coupled-column formats.[5,6] In such a system, species do not simply separate along a single linear dimension but over an area defined by the two separation mechanisms. Assuming unit resolution between neighboring peaks,[3] a nondimensional quantity known as the peak capacity of a 1D separation, n, can be expressed as

$$n = L/w \propto \sqrt{N} \tag{1}$$

Here L is the separation channel length and w is a measure of the average analyte bandwidth based on the standard deviation of the concentration distribution, σ. Typical estimates of w include 4σ and the full width half-maximum value (for a Gaussian distribution, fwhm $\approx 2.35\sigma$). The peak capacity is proportional to the square root of the number of theoretical plates ($N = L^2/\sigma^2$). The total peak capacity of a 2D system, n_{total}, is estimated to be the product of the peak capacities of each respective separation dimension,[2]

$$n_{total} = n_1 n_2 \tag{2}$$

where n_1 and n_2 are the peak capacities of the constituent separation dimensions, as described in eq 1. Giddings outlined considerations for discrete coupling of techniques that include the independence of each successive separation mechanism (orthogonality), rapid peak generation, high resolution, and overall technique compatibility.[2] Isoelectric focusing (IEF) coupled with gel or free solution electrophoresis generally satisfies these conditions and has been employed in the analysis of complex samples on the macroscale for some time.[4,7] During such a 2D analysis, the initial IEF step comes to completion, is halted, and a subsequent electrophoretic analysis proceeds. With its demonstrated high resolving power, slab-gel 2D electrophoresis is considered a workhorse of proteomic research. Although crucial to such research, the technique is a bottleneck that can take as much as three working days to complete.[1,8] While automation would speed the process considerably, miniaturization and the use of microfabricated devices begins to address throughput requirements through decreased analysis times.[9,10]

* Corresponding author: (voice) 925-294-3738; (fax) 925-294-3738; (e-mail) aeh@stanfordalumni.org.

† Department of Mechanical Engineering.

‡ Present address: Sandia National Laboratories, Livermore, CA 94551-9951.

§ Present address: Caliper Technologies Corp., Mountain View, CA 94043-2234.

∥ Department of Medicine.

⊥ Department of Chemical Engineering.

(1) Mouradian, S. *Curr. Opin. Chem. Biol.* **2002**, *6*, 51−56.
(2) Giddings, J. C. *Anal. Chem.* **1984**, *56*, 1258A−1270A.
(3) Giddings, J. C. *Unified Separation Science*; Wiley: New York, 1991.
(4) O'Farrell, P. H. *J. Biol. Chem.* **1975**, *250*, 4007−4021.
(5) Bushey, M. M.; Jorgenson, J. W. *Anal. Chem.* **1990**, *62*, 978−984.
(6) Giddings, J. C. In *Multidimensional Chromatography: Techniques and Applications*; Cortes, H. J., Ed.; Marcel Dekker: New York, 1990; pp 1−27.
(7) Klose, J. *Humangenetik* **1975**, *26*, 231−243.
(8) Berkelman, T.; Stenstedt, T. *Amersham Biosciences Handbook*; 80-6429-60.
(9) Hille, J. M.; Freed, A. L.; Watzig, H. *Electrophoresis* **2001**, *22*, 4035−4052.
(10) Khandurina, J.; Guttman, A. *J. Chromatogr., A* **2002**, *943*, 159−183.

10.1021/ac026239a CCC: $25.00
Published on Web 01/25/2003

Single-dimension separations are today commonly performed on-chip. Examples of demonstrated on-chip 1D separations include capillary electrophoresis (CE),[11−13] open channel electrochromatography (OCEC),[14] micellar electrokinetic chromatography (MEKC),[15] and IEF.[16−19] In contrast, few on-chip 2D separation development efforts have been reported, with the exception of separations coupled to mass spectroscopy as described by Khandurina and Guttman and references therein.[10] In an effort to integrate several steps on a single device, Bousse et al. have developed a method for fast on-chip fluorescence labeling and sizing of proteins.[20] As for integrated on-chip separations, Rocklin et al.[21] and Gottschlich et al.[22] have sequentially coupled chromatographic techniques (MEKC and OCEC, respectively) with CE. While investigation of OCEC−CE showed a lack of orthogonality in some instances, MEKC−CE was shown to be an efficient separation scheme with a good system peak capacity (n_{total} of 500−1000, based on fwhm). While these 2D on-chip separations were conducted in liquid phase, the composition of the medium was varied between the first and second dimensions. A key feature of the on-chip IEF−CE system described in this work is the initial uniformity of the separation media in both dimensions. In this system, control of the reservoir conditions at the terminus of each dimension (e.g., pH, applied potential) determines the electrophoretic separation mechanism acting in the microchannel (i.e., IEF or CE).

IEF is attractive as the first dimension of a microdevice-based separation for several reasons. Namely, the focusing nature of IEF increases species concentrations substantially from that of the initial sample mixture—concentration increases of a 100-fold are common using capillary-based IEF.[23] This concentrating of the sample improves the detection limits of a miniaturized system, making CE separations in the second dimension feasible for initially dilute sample concentrations. Unlike CE, the focusing behavior also makes the technique insensitive to injection dispersion present in an initial sample plug. Additionally, due to the short length scales employed, the speed with which miniaturized IEF separates species is substantially faster than that of conventional capillary or slab-based separations.[16,18,24] Last, the persistence of focused sample bands and the ability to defocus and readily refocus those bands is attractive for on-chip 2D devices.[25] These latter two characteristics allow flexibility in system design, as the time necessary for sample handling and subsequent separation in the second dimension does not result in degraded resolution or signal in the IEF dimension.

IEF is typically implemented using a mobilization force to transport focused sample species past a single-point detector. While full-field imaging renders mobilization for detection purposes unnecessary,[26] the need to further manipulate or fractionate focused species may benefit from mobilization. An EOF mobilization approach was developed for use in fused-silica capillaries using various dynamic channel coatings.[27−29] Hofmann et al. adapted this "one-step" EOF mobilization technique for use in quartz microdevices.[16] In the quartz microdevice study, no coatings were used, thus resulting in short species residence times within the separation channel. Microchannels fabricated in acrylic substrates exhibit electroosmotic mobilities lower than those measured in glass capillaries.[30] For applications that require fine handling of focused sample bands for further analysis, such as the IEF−CE system considered in this work, a slow nondispersive mobilization method could prove useful.

The current work details development of a microfluidic platform that sequentially couples liquid-phase IEF and free solution electrophoresis (CE). Fluorescent species are separated by IEF in the first dimension and CE in the second. The separation medium in each dimension is a mixture of ampholytes (focused ampholytes for IEF and unfocused ampholytes for CE). Full-field CCD imaging is used as a tool for the design and characterization of the device. The 2D on-chip separation method is compared to independent relevant 1D on-chip separations.

EXPERIMENTAL SECTION

Chemicals and Instrumentation. Bio-Lyte pH 3−10 carrier ampholytes at 2% w/v (BioRad Laboratories, Hercules, CA) were used as the liquid-phase separation medium for all separation experiments. For the IEF experiments, 40 mM sodium hydroxide at pH 10 (Catalog No. 148-5028, BioRad) was used as the catholyte and 20 mM phosphoric acid at pH 3 (Catalog No. 148-5029, BioRad) was used as the anolyte. All channels were rinsed with filtered (0.2-μm pore size) 1 M sodium hydroxide for ∼5 min before and after use. Following the sodium hydroxide rinse, channels were washed with deionized water and air for 2 min. All channels were stored dry. Recombinant green fluorescent protein (GFP, MW 26 900) (Catalog No. AFP5201, Q Biogene, Montreal, PQ, Canada), FITC-labeled dextran (MW 10 000), and FITC-labeled ovalbumin (MW 45 000−46 000) were used for the experiments presented here. Sample concentrations were in the

(11) Harrison, D. J.; Fluri, K.; Seiler, K.; Fan, Z. H.; Effenhauser, C. S.; Manz, A. *Science* **1993**, *261*, 895−897.
(12) Effenhauser, C. S.; Manz, A.; Widmer, H. M. *Anal. Chem.* **1993**, *65*, 2637−2642.
(13) Jacobson, S. C.; Hergenroder, R.; Koutny, L. B.; Ramsey, J. M. *Anal. Chem.* **1994**, *66*, 1114−1118.
(14) Jacobson, S. C.; Hergenroder, R.; Koutny, L. B.; Ramsey, J. M. *Anal. Chem.* **1994**, *66*, 2369−2373.
(15) Moore, A. W.; Jacobson, S. C.; Ramsey, J. M. *Anal. Chem.* **1995**, *67*, 4184−4189.
(16) Hofmann, O.; Che, D.; Cruickshank, K. A.; Müller, U. R. *Anal. Chem.* **1999**, *71*, 678−686.
(17) Mao, Q. L.; Pawliszyn, J. *J. Biochem. Biophys. Methods* **1999**, *39*, 93−110.
(18) Herr, A. E.; Molho, J. I.; Santiago, J. G.; Kenny, T. W. *Technical Digest of the 2000 Solid-State Sensor and Actuator Workshop*; Hilton Head Island, SC, Transducers Research Foundation; 2000; pp 115−119.
(19) Macounova, K.; Cabrera, C. R.; Holl, M. R.; Yager, P. *Anal. Chem.* **2000**, *72*, 3745−3751.
(20) Bousse, L.; Mouradian, S.; Minalla, A.; Yee, H.; Williams, K.; Dubrow, R. *Anal. Chem.* **2001**, *73*, 1207−1212.
(21) Rocklin, R. D.; Ramsey, R. S.; Ramsey, J. M. *Anal. Chem.* **2000**, *72*, 5244−5249.
(22) Gottschlich, N.; Jacobson, S. C.; Culbertson, C. T.; Ramsey, J. M. *Anal. Chem.* **2001**, *73*, 2669−2674.
(23) Shen, Y. F.; Berger, S. J.; Anderson, G. A.; Smith, R. D. *Anal. Chem.* **2000**, *72*, 2154−2159.
(24) Raisi, F.; Belgrader, P.; Borkholder, D. A.; Herr, A. E.; Kintz, G. J.; Pourhamadi, F.; Taylor, M. T.; Northrup, M. A. *Electrophoresis* **2001**, *22*, 2291−2295.
(25) Herr, A. E.; Molho, J. I.; Bharadwaj, R.; Santiago, J. G.; Kenny, T. W.; Borkholder, D. A.; Northrup, M. A. *Proceedings of the uTAS 2001 Symposium*, Monterey, CA; Kluwer Academic Publishers: New York, 2001; pp 51−53.
(26) Wu, X. Z.; Wu, J. Q.; Pawliszyn, J. *Electrophoresis* **1995**, *16*, 1474−1478.
(27) Mazzeo, J. R.; Martineau, J. A.; Krull, I. S. *Anal. Biochem.* **1993**, *208*, 323−329.
(28) Thormann, W.; Caslavska, J.; Molteni, S.; Chmelik, J. *J. Chromatogr.* **1992**, *589*, 321−327.
(29) Mazzeo, J. R.; Krull, I. S. *Anal. Chem.* **1991**, *63*, 2852−2857.
(30) Caslavska, J.; Thormann, W. *J. Microcolumn Sep.* **2001**, *13*, 69−83.

100−200 nM range and were stored chilled (20 °C) after dilution with the carrier ampholytes.

Characterization of Analytes. For comparison with the microfluidic device, slab-gel IEF was performed on the sample species. Precast immobilized pH gradient (IPG) gel strips with a linear pH gradient range of 3−10 were rehydrated overnight in rehydration buffer (8 M urea, 4% CHAPS, 10 mM DTT, 0.2% (w/v) Bio-Lyte 3−10) containing sample. Focusing was performed using the BioRad Protean IEF cell for a total of 6 h at 20°C. A mixture of 2D SDS−PAGE standards (BioRad) was used as a calibrated p*I* reference. Gels were stained with Bio-Safe Coomassie (BioRad) and visualized by scanning using a BioRad Molecular imager FX Pro Plus (BioRad).

Microdevice Imaging Technique. The species transport was observed using standard epifluorescence techniques and a CCD camera. During the separations, the fluorescent sample species were excited with a mercury lamp using epifluorescence filter sets for GFP (Omega Optical Inc., Brattleboro, VT). Images were collected using an inverted epifluorescence microscope (IX-70, Olympus, Melville, NY) equipped with 2×, 4×, and 10× objectives (numerical apertures of 0.08, 0.16, and 0.4, respectively). An *x*−*y* translation stage (Olympus, Melville, NY) was used to position the chip and fixturing relative to the imaging optics. A 0.31× demagnifier (Diagnostic Instruments Inc., Sterling Heights, MI) was used to increase the field of view projected onto the CCD. A 1300 × 1030, Peltier-cooled interline CCD camera (MicroMax 1300YHS, Roper Scientific, Trenton NJ) was employed for image collection. A typical sampling rate of 2 Hz was used with image capture coordinated using a digital delay generator (Berkeley Nucleonics Corp., San Rafael, CA). Subsequent image analysis was conducted using a combination of in-house Matlab image processing code (The Math Works Inc., Natick, MA) and available and in-house Java plug-ins developed using ImageJ (National Institutes of Health, Bethesda, MD, http://rsb.info.nih.gov/ij/). Images were corrected for background signal and normalized to adjust for spatial nonuniformities in the excitation and collection efficiencies. Peak width and relative position were computed from spatial electropherograms obtained by binning each CCD image in a direction perpendicular to the particular separation axis.

Microchip Device and 2D IEF−CE Device Operation. Custom planar microchips were designed in-house and then fabricated by Aclara Biosciences (Mountain View, CA) in poly(methyl methacrylate) (acrylic) using an imprinting and laminating technique similar to that reported in the literature.[31] Microchannels fabricated in acrylic were selected because of the low electroosmotic mobility associated with the microchannel walls, as compared to the mobility of untreated glass substrates.[30,32] To fabricate the microdevice, a wet-etched glass plate (mold master) was electroplated to create a metal electroform (mold tool). The mold tool was then used to emboss an acrylic substrate, creating grooves that were subsequently sealed with a thin acrylic laminate to form the enclosed microchannels. Fluidic and electrical access holes were drilled in the acrylic substrate prior to the laminate sealing step. The channel cross sections were D-shaped, as is characteristic of the isotropic etch used in the mold-making procedure, and measured 200 μm wide by 20 μm deep. For the 1D IEF, a straight channel (length of 2.54 cm) was used. A cross geometry was used for both the 1D CE and the 2D studies. The cross geometry had a horizontal channel length of 2.8 cm and an intersecting vertical channel of length 2.5 cm. Custom fixturing was designed and fabricated in-house to provide wells for inserting electrodes and allow for pressure filling of liquid into the channels.

An important aspect of our liquid-phase approach is the use of an initially uniform ampholyte buffer solution in both the IEF and CE dimensions. IEF and CE are achievable in the same ampholyte buffer solution through control of the chemistry and applied potential at the reservoirs. Pressure-driven flow was used initially to fill all channels with the ampholyte solution. Electrokinetic flow was subsequently used to fill only the IEF channel with the sample mixture. After the channels were filled, excess sample was removed from the anolyte and catholyte reservoirs. To prevent mobilization of the sample out of the IEF channel, the anolyte and catholyte reservoirs were simultaneously filled with electrolyte using two pipets. Platinum electrodes were submerged in the fluid of each reservoir, and high voltage was applied and adjusted using a computer-controlled high-voltage power supply (Micralyne, Edmonton, AB, Canada). The ampholytes in the IEF dimension, with acidic and basic boundary conditions at the terminal reservoirs, aligned under an applied axial electric field to form an axial pH gradient. Focused species were mobilized, using EOF, to an intersection where fluidic volumes from the first dimension (IEF) were electrokinetically sampled into the second dimension (CE). In the CE dimension, the ampholytes lacked the extreme pH boundary conditions and, thus, remained unfocused—behaving as a buffer with a measured pH of 8.5.

RESULTS AND DISCUSSION

In this section, we first present an examination of on-chip IEF in low-viscosity ampholytes. Next, we present results for an ampholyte-based CE separation technique. Last, we present a 2D assay that integrates these two processes on a single microfluidic device.

On-Chip 1D IEF. During steady-state IEF, the variance of focused concentration distributions can be expressed in terms of species properties and system operating conditions.[33] The variance has an inverse dependence on the applied electric field strength, E, and the steepness of the pH gradient, dpH/dx,

$$\sigma^2 = \frac{C_1}{E\ \mathrm{dpH}/\mathrm{d}x} \tag{3}$$

Properties specific to the sample species have been grouped as $C_1 = D/[-\mathrm{d}\mu/\mathrm{d}(\mathrm{pH})]$, where D is the diffusivity of the species and μ is the electrophoretic mobility of the species. From eq 3, it is apparent that the variance of the focused distributions will decrease as either the steepness of the pH gradient (dictated by the pH boundary conditions and channel length) or the strength of the applied electric field is increased. To investigate the relationship between the applied field strength and the characteristic focused zone width in our 1D IEF microsystem, a sample

(31) Boone, T. D.; Hooper, H. H.; Soane, D. S. *Technical Digest of the 1998 Solid-State Sensor and Actuator Workshop*, Hilton Head, SC, Transducers Research Foundation; 1998; pp 87−92.

(32) Locascio, L. E.; Perso, C. E.; Lee, C. S. *J. Chromatogr., A* **1999**, *857*, 275−284.

(33) Catsimpoolas, N. *Isoelectric Focusing*; Academic Press: New York, 1976.

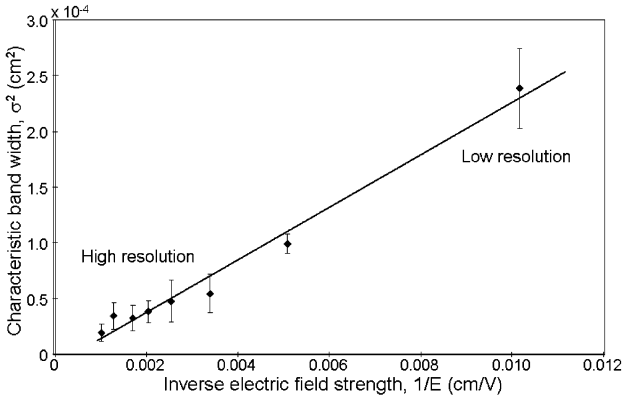

Figure 1. Spatial variance of the predominant GFP peak at various applied field strengths for 1D on-chip IEF. The data (solid points) are shown with a least-squares fit (solid line) to a $1/E$ behavior ($R^2 = 0.97$). The *y*-axis error bars represent the maximum scatter in run-to-run reproducibility, with three to six measurements at each field strength.

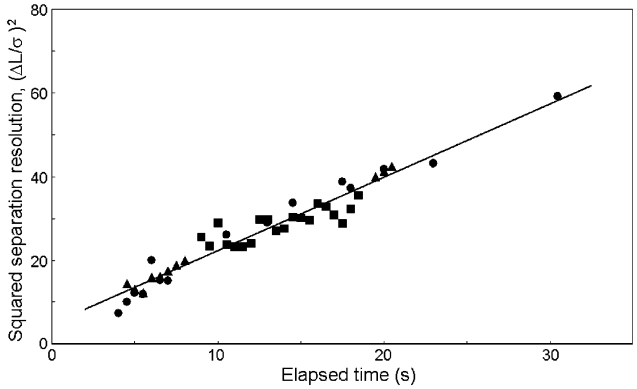

Figure 2. Time-dependent squared separation resolution, $SR^2 = (\Delta L/\sigma)^2$, during 1D ampholyte-based CE. Shown are three independent experiments (squares, circles, triangles), conducted at $E = 315$ V/cm, having a linear correlation coefficient of 0.94.

solution consisting of only GFP was focused at a variety of field strengths and the variance of the resulting concentration distributions was measured. These results are shown in Figure 1. A least-squares fit shows σ^2 varies linearly with $1/E$ ($R^2 = 0.97$) for a given initial sample mass, as would be expected in IEF. In such experiments, Joule heating limits the maximum resolution at higher applied field strengths.[34] The error bars in Figure 1 show the run-to-run reproducibility of the data and were estimated using between three and six realizations. Sources of variation include pressure-driven flow in the IEF channel (arising from slight fluid height differences between the reservoirs, meniscus shape differences between the reservoirs, or both) and background noise in the intensity signal. Using eq 1 to estimate the peak capacity of the system yields $n \sim 146$ ($w = 174$ μm) at $E = 295$ V/cm and $n \sim 175$ at $E = 495$ V/cm ($w = 145$ μm) for the 1D IEF system. The latter peak capacity shows improvement over that calculated from the reported N for a similar separation on a quartz microchip (from eq 1, a plate number of $N = 27\,000$ gives $n_{IEF} = (1/2.35)27000 = 70$ at 500 V/cm).[16] All species were present in concentrations of 150 nM prior to focusing. Based on the channel length ($L = 2.54$ cm) and the largest final focused zone width ($4\sigma = 350$ μm), the sample species are estimated to have concentrated by a factor of 73, resulting in a final focused concentration of $\sim$10 μM.

The velocity of the focused GFP species was continuously monitored and used as a measure of the mobilization velocity in the IEF channel during the 1D separation process. Focusing and detection took place in less than 60 s, with focused species bands initially detectable within 15 s. The applied electric potential was periodically removed, and the resultant peak drift velocities were recorded to correct for low bulk fluid flow imparted by pressure-head or meniscus differences between the channel reservoirs. The measured mobility of the GFP band decayed with time, with the mobility at the start of IEF ($\mu_{mob} = 0.3 \times 10^{-4}$ cm^2/V·s) being a factor of 7.5 higher than the mobility measured 10 min later ($\mu_{mob} = 0.04 \times 10^{-4}$ cm^2/V·s). The mobilities measured in the microdevice IEF system during electroosmotic mobilization were 8-fold smaller than electroosmotic mobilities reported for PMMA capillaries filled with phosphate buffer (pH 8.5, $\mu = 2.5 \times 10^{-4}$ cm^2/V·s)[30] (the mobilities measured near the end of mobilization were 62-fold smaller than the value reported for PMMA). Other IEF studies have noted possible EOF suppression when focused carrier ampholyte solutions are used.[35, 36]

In general, electrokinetic separation systems with nonuniform ζ-potential distributions result in velocity distributions that are not pluglike in nature. The variation in the ζ-potential gives rise to induced pressure gradients and associated advective dispersion.[37] Although the axial pH gradient required for IEF may result in ζ-potential variation, the mobilized IEF bands do not display increased dispersion. Based upon properties reported for PMMA,[30] the magnitude of the induced pressure-driven flow in our IEF system is expected to be on the order of the measured electroosmotic mobilization velocity, ($U_{pressure} \sim 20$ μm/s). This velocity is such that the time required for a molecule to diffuse across the depth, d, of the microchannel (d^2/D) is on the order of the time required for a molecule to advect by pressure-driven flow the same distance ($d/U_{pressure}$). This condition results in minimal advective dispersion.[38] Furthermore, any dispersion arising from induced pressure-driven flow will be obscured by the focusing effect of IEF. These two conditions explain the observation of low dispersion band transport during the IEF step. A nondispersive mobilization scheme, such as the slow EOF mobilization used in this system, is important for maintaining high resolution during the IEF portion of the analysis.

On-Chip 1D Ampholyte-Based CE. Ampholyte-based 1D CE experiments were conducted on the GFP sample analyzed in the 1D IEF study using the minimum dispersion injection scheme developed by Alarie et al.[39] The CE analysis revealed three peaks present in the GFP sample, as will be further discussed in the next section. The separation resolution, $SR^2 = \Delta L^2/\sigma^2$ (based on the major and flanking peaks), was measured to investigate the

(34) Grushka, E.; McCormick, R. M.; Kirkland, J. J. *Anal. Chem.* **1989**, *61*, 241−246.
(35) Tang, Q.; Lee, C. S. *J. Chromatogr., A* **1997**, *781*, 113−118.
(36) Xu, J. D.; Locascio, L.; Gaitan, M.; Lee, C. S. *Anal. Chem.* **2000**, *72*, 1930−1933.
(37) Herr, A. E.; Molho, J. I.; Santiago, J. G.; Mungal, M. G.; Kenny, T. W.; Garguilo, M. G. *Anal. Chem.* **2000**, *72*, 1053−1057.
(38) Dutta, D.; Leighton, D. T. *Anal. Chem.* **2001**, *73*, 504−513.
(39) Alarie, J. P.; Jacobson, S. C.; Culbertson, C. T.; Ramsey, J. M. *Electrophoresis* **2000**, *21*, 100−106.

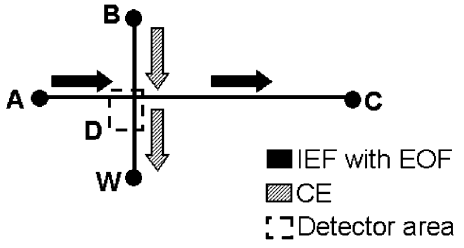

		Duration (s)	Reservoir: A	C	B	W
n repeats	IEF/EOF	6 - 10	HV	G	F	F
	Sampling	3	F	F	F	F
	CE	32	F	F	G	HV

Figure 3. Separation algorithm for the 2D IEF−CE separation. The device geometry is shown with arrows indicating the sample motion during each serial separation step. The first dimension (IEF) extends from reservoir A (anolyte) to reservoir C (catholyte). The second dimension (CE) extends from reservoir B (buffer) to reservoir W (waste). The imaged area is indicated by the dashed box, D. The voltage applied during each step of the 2D separation is shown in the table (HV, high voltage; G, ground; F, float).

behavior of unfocused ampholytes as the CE buffer. Figure 2 shows the behavior of SR^2 for three independent separations along with a linear least-squares fit to the data ($R^2 = 0.94$). In general, CE separations exhibit a linear increase in the SR^2 value with time due to constant velocity differences between species and linear increases in band variance with time. In contrast, during the steady-state phase of IEF, sample bands do not move relative to each other nor do they broaden due to diffusion resulting in a constant SR^2 value. The linear dependence on time exhibited by the measured SR^2 values presented in Figure 2 is consistent with a CE separation mechanism, thus indicating that CE can be performed on-chip in a solution of unfocused ampholytes. The ability to perform CE in unfocused ampholytes enables coupling of liquid-phase IEF to ampholyte-based CE in the IEF−CE system detailed in this work.

On-Chip IEF−CE. The experiments described above are a demonstration and characterization of on-chip IEF and on-chip ampholyte-based CE. In this section, we present an on-chip separation that sequentially combines IEF and CE in a single device. The microchip geometry shown in Figure 3 was used, and the arrows in the figure indicate the direction of sample movement during each separation. The table in Figure 3 and the CCD images presented in Figure 4 aid in description of the 2D separation algorithm. After the initial focusing step, the 2D separation algorithm consisted of multiple iterations through the following sequence of steps: (Figure 4A) an IEF separation with simultaneous EOF mobilization of sample species along the axis of the first dimension (IEF/EOF), (Figure 4B) electrokinetic sampling of a relatively small volume of the IEF dimension constituents into the CE channel, and (Figure 4C) a CE separation in the second dimension. Figure 4D shows the start of the next separation cycle in which IEF and simultaneous mobilization have been reinitiated in the first dimension. As this is a serially implemented 2D separation, the separation sequence is repeated until all fluid volumes from the IEF dimension have been sampled into the CE dimension.

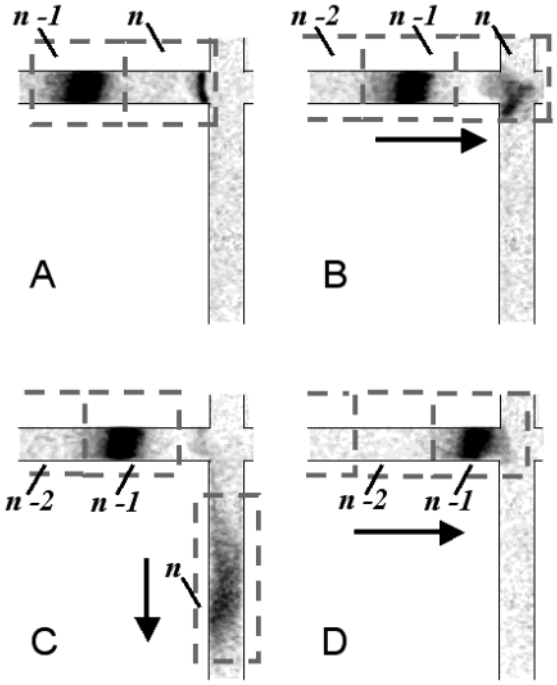

Figure 4. CCD images during species sampling. (A) Species are focused by IEF in the first dimension (dark bands in horizontal channel). Simultaneously, the bands are mobilized toward the catholyte reservoir by low-dispersion EOF. (B) Once a fluid volume of interest, *n*, reaches the microchannel intersection, all electrodes are switched to electrically float for 3 s. (C) High voltage is then applied at reservoir B and reservoir W is grounded, initiating sample separation in the second dimension. (D) Upon completion of the CE separation, IEF/EOF is reinitiated causing sample species to refocus and the next fluidic volume ($n - 1$) to migrate to the intersection. This sequence is repeated until all fluidic volumes are sampled from first dimension into the second.

Simultaneous focusing and EOF-driven mobilization transported focused sample species to the sampling intersection with an electroosmotic velocity of order 20 μm/s (Figure 4A, D). After a fluidic volume of interest reached the intersection (Figure 4B), all reservoirs were switched to electrically float for 3 s prior to sampling. During this period, focused sample species began to defocus, as presumably did the much lower molecular weight ampholytes. The floating step was incorporated into the voltage algorithm to electrically decouple the two assay dimensions and to allow for a more homogenized pH field near the intersection. Mass continuity ensures that the bulk of fluid sampled from the IEF dimension into the CE dimension was replaced with unfocused ampholyte solution (Figure 4C). This algorithm resulted in an IEF separation that was essentially "parked" during each CE analysis, as species were refocused ($E = 350$ V/cm for 6−10 s) prior to additional CE analyses (Figure 4D). Each sampling event, CE separation, and IEF refocus cycle had a period of 45 s.

Figure 5 shows the intensity signal from a region of the IEF dimension before and after the single sampling event shown in the CCD images in Figure 4. The shaded portion of the electropherogram corresponds to the volume fraction sampled from the IEF dimension into the CE dimension. After sampling of the shaded peak, the remaining species were refocused in preparation for continued sampling. Note that the sample intensity distribution in the $x/L_{image} < 0.7$ region of the image is largely undisturbed,

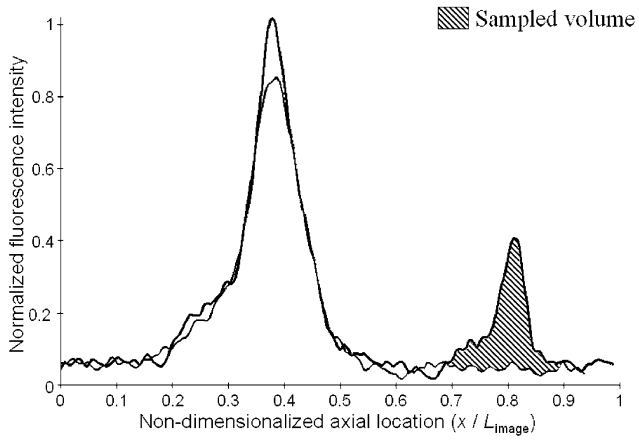

Figure 5. Sampling resolution for 2D separation. A spatial electropherogram is shown for the IEF dimension prior to species sampling (black line) and after sampling (gray line) during the sampling event shown in Figure 4. The shaded area is the difference between the intensity signals and corresponds to the volume sampled from the IEF dimension into the CE dimension. IEF was not reinitiated prior to acquisition of the "after sampling" electropherogram; thus, the high-intensity peak ($x/L_{image} \sim 0.4$) has decayed in intensity due to diffusional broadening. Once IEF is reinitiated, the peak height is regained. The high-intensity peak indicates detection of an initial sample mass of 0.05 μg and arises from the GFP sample. The right-most peak is the FITC-dextran sample.

indicating that only a small fraction of the IEF fluid volume was introduced into the CE channel. Figure 5 shows that it is possible to sample all fluid volumes from the first dimension into the second due to the near stationary nature of the species remaining in the first dimension during an analysis in the second dimension. It is important to note that species are effectively mixed to the length scale of the junction geometry during the sampling process, as the width of the CE channel approximately defines the resolution available from the first dimension. To fully optimize a multidimensional system, each effluent peak from the first dimension should be sampled into the second dimension several times, as described by Murphy et al.[40] This "oversampling" of peaks from the first dimension into the second enhances the overall separation resolution of a 2D system. Further improvements to this system are necessary in order to ensure oversampling of all species (e.g., reduced sampled volume widths along the IEF dimension).

Two-dimensional "gel-like" plots were constructed from a time sequence of CCD images collected during the 2D separations. The gel-like plots were formatted to display inverted gray scale intensity information to mimic a slab-gel result with dark regions corresponding to high fluorescence intensity zones. Figure 6 shows the results of a 2D separation using a gel-like format for three time steps during the 2D analysis (Δt of 3, 5, and 7s). Each vertical column ("lane") in the gel-like plot is generated from a spatial electropherogram that indicates the intensity of fluorescence along the CE separation channel. In each gel-like plot, the electropherograms correspond to equal duration CE separations (i.e., the CE data for each 2D plot were collected at equal time periods after the respective electrokinetic injection). Accordingly, the ordinate axis of the gel-like plot corresponds to the axial coordinate along the second dimension of the assay. Since the method developed in this work is a serial 2D analysis, the vertical lanes correspond to CE analyses of fluid volumes sampled from different, adjacent locations along the IEF dimension; thus, each vertical lane is an analysis of a single sampling event from a discrete pI range. As a consequence, the abscissa of each 2D plot is proportional to the axial dimension along the IEF channel. Recall that, during IEF, the focused bands are mobilized from left to right into the injection region with a mobilization velocity of roughly 20 μm/s. The left-most lane of each gel-like plot presented in Figure 6 corresponds to the first sampling event, while columns to the right correspond to subsequent sampling from fluid volumes containing decreasing pI values.

Using the spatially and temporally varying intensity data, species were identified in Figure 6 using relative pI locations and apparent mobilities. The apparent mobilities for species analyzed by the 2D system were calculated from velocities measured during species analysis in the second dimension. Table 1 shows the resulting agreement between apparent mobilities measured during the CE portion of IEF−CE and mobilities measured using on-chip 1D ampholyte-based CE. A Student's t distribution was used to estimate the error in measured mobilities within a 95% confidence interval (four trials for FITC-dextran and five for the other two species). The mobilities measured using 1D CE and 2D IEF−CE agree reasonably well. Variation in measured mobilities could arise from differences in the background bulk flow (i.e., pressure-driven or electroosmotic flow) between the experiments. Adsorption of the FITC-dextran to the microchannel walls may explain the large variation in the measured mobility. Figure 7 shows the time-dependent motion of the center of mass for each identified species. The measurements indicate a linear dependence of center of mass location on time ($R^2 > 0.99$). The variance of sample plugs also increased linearly with time ($R^2 > 0.94$) during analysis in the second dimension. Each behavior is consistent with a CE mechanism acting in the second dimension to within the temporal resolution of the experiment (0.5 s).

A central goal of any 2D separation system is the ability to separate and detect species not detectable by independent 1D separations. The 2D analysis shown in Figure 6 meets this goal by resolving species not identified during companion on-chip 1D separations under similar experimental conditions ($E_{IEF} = 350$ V/cm and $E_{CE} = 395$ V/cm). These unidentified peaks are labeled numerically (i.e., 1, 2, and 3) in Figure 6. The unidentified peaks are postulated to be associated with the GFP and FITC−ovalbumin samples. This hypothesis is supported by the work of Richards et al. in which three GFP bands were detected using slab-gel IEF analysis.[41] Slab-gel IEF analysis of the samples used in the current study also confirmed the presence of three species ($pI_1 = 5.9$, $pI_2 = 6.1$, $pI_3 = 6.4$), as well as the presence of multiple species in the FITC−ovalbumin sample (numerous unresolved species having pI values between 5.0 and 5.3).

Overall system peak capacity and throughput are important performance metrics for any analysis system. Based on a conservative estimate of the standard deviation of a sampled peak at the detector ($\sigma = 520$ μm for $E = 395$ V/cm) and the 1.3-cm channel length, the CE dimension has a peak capacity, based on fwhm, of

(40) Murphy, R. E.; Schure, M. R.; Foley, J. P. *Anal. Chem.* **1998**, *70*, 1585−1594.

(41) Richards, D. P.; Stathakis, C.; Polakowski, R.; Ahmadzadeh, H.; Dovichi, N. J. *J, Chromatogr., A* **1999**, *853*, 21−25.

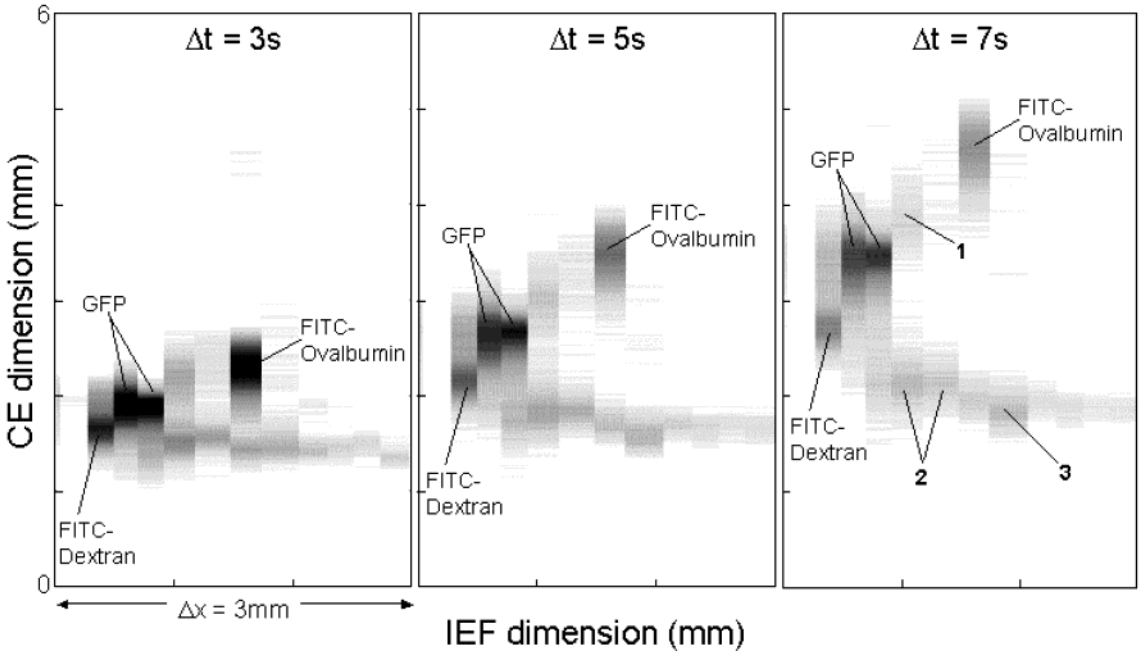

Figure 6. Gel-like plots of an IEF−CE separation at CE analysis times of 3, 5, and 7 s. The horizontal axis corresponds to the relative position of each fluid element during the IEF separation. Approximately 3 mm, or 15%, of the total IEF channel length was sampled ($E = 350$ V/cm). The vertical axis corresponds to the spatial axial dimension of the subsequent CE separations ($E = 390$ V/cm). Species not identified in companion 1D separations are labeled as peaks 1, 2, and 3.

Table 1. Measured Apparent Mobilities for the Predominant Sample Species

	mobility, $\mu \times 10^4$ cm^2/V·s	
	1D CE (on-chip)	2D IEF−CE (on-chip)
FITC-ovalbumin	−1.3 ± 11%	−1.4 ± 7%
GFP	−1.0 ± 15%	−1.0 ± 6%
FITC-dextran	−0.4 ± 57%	−0.7 ± 18%

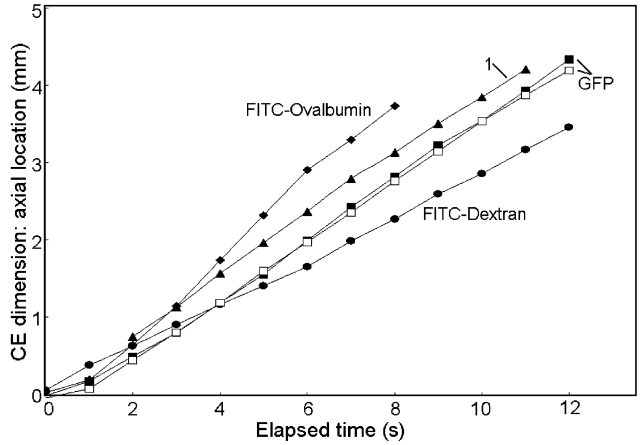

Figure 7. Mobility behavior for predominant species during the CE portion of the IEF−CE separation. Mobilities are tabulated in Table 1; species labels are consistent with Figure 6. All species exhibited linear correlation coefficients of greater than 0.992. The two measurement sequences marked as GFP were collected from neighboring CE lanes and indicate oversampling of that species.

~10. The peak capacity of 1D IEF is a function of the applied electric field strength (as indicated by the behavior of the focused band variance shown in Figure 1). However, in the 2D system, the effective peak capacity of the IEF dimension is limited by the spatial resolution of the sampling junction. In the current 2D system, this spatial resolution is ~200 μm (one channel width) resulting in an effective $n \sim 130$ for the IEF dimension. Combining the IEF peak capacity estimate with that of the CE dimension, eq 2 yields an estimated overall 2D system peak capacity of 1300. This peak capacity estimate compares favorably with the estimated peak capacity of the MEKC−CE system described by Rocklin et al. (500−1000 based on fwhm).[21] As further comparison, peak capacities for standard gel 2D electrophoresis are in the 1000−3000+ range.[9] The peak capacity of our system could be improved by lengthening the CE separation channel (for greater CE separation efficiency, assuming the assay is not signal limited), employing CE channels that have a smaller channel width to characteristic species bandwidth ratio (to increase the effective peak capacity of the first dimension), and through precise control of pressure-driven flow in all channels at the sampling junction (which would reduce injection dispersion). The data presented in Figure 6 represent sampling from a fluid volume that occupies ~15% of the IEF dimension—the region of the IEF channel that contained the sample species and, thus, exhibited measurable signal. The initial focusing, mobilization, sampling, and separation in the second dimension of this targeted region were completed in less than 5 min. Based on these measurements, use of this geometry (e.g., a single channel comprising the second dimension) should yield a 2D analysis of nearly 100% of the first-dimension volume in less than 1 h.

CONCLUSIONS

We have demonstrated a single, planar, polymer microdevice that serially integrates two rapid, orthogonal chip-based separation schemes (IEF and CE). The boundary conditions of the terminal channel reservoirs (e.g., applied potential, chemistry, and pH) in a cross geometry were used to govern the separation mechanisms

throughout the analysis. A mixture of fluorescent sample species was focused during IEF and mobilized by low-dispersion EOF to a junction, where effluent volumes were repeatedly electrokinetically sampled into the CE dimension. Such electrokinetic control of sample species and bulk fluid motion is advantageous for automated on-chip systems. Comparison of the 2D system behavior to that of the 1D constituent separation mechanisms showed good agreement. IEF in both the 1D and 2D systems showed rapid peak generation (less than 1 min), reduced EOF without the introduction of high-viscosity additives, resultant highly concentrated sample species (70-fold), and a high peak capacity. Species behavior in the second dimension of the IEF−CE system was consistent with a CE separation mechanism (i.e., a constant velocity difference between neighboring peaks and diffusional broadening of injected sample species). These results suggest that the two separation mechanisms (IEF and CE) remain independent despite the fact that the two separation dimensions are fluidically coupled and use the same liquid medium. Results from the 2D analysis suggest increased separation resolution over that of the corresponding uncoupled 1D separations, as peaks that were not detectable during 1D separations under identical conditions were apparent in the 2D separation. The complete 2D system was estimated to have a peak capacity of ∼1300.

The peak capacity and resolution may be further improved by reducing the size of each fluid volume sampled into the second dimension (perhaps by reducing the width of the sampling junction), increasing the channel length of the second dimension, and reducing dispersion during sample handling between the first and second dimensions. The low viscosity of the separation media, in combination with the short separation channel length scales used, resulted in rapid IEF and CE analyses. That noted, the analysis time of this system was dominated by that of the second dimension and could be reduced further through implementation of a manifold of CE channels that would allow sampling and analysis of numerous analyte volumes from the first dimension in parallel. The total analysis time for a parallel system should decrease as the number of additional CE channels increases, although system complexity will also increase. The liquid-phase approach presented here may facilitate further system integration, including fraction collection and coupling of IEF−CE with a third dimension (e.g., mass spectrometry).

ACKNOWLEDGMENT

The authors acknowledge Aclara Biosciences (Mountain View, CA) for chip fabrication. The authors also acknowledge Dr. Anup Singh at Sandia National Labs (Livermore, CA) for the fluorescently labeled ovalbumin sample. During portions of this work, A.E.H. was supported by a National Science Foundation Graduate Research Fellowship and J.I.M. was supported by a Hewlett-Packard Stanford Graduate Fellowship. This work was supported in part by grants from NIH (5U19 AI50864, 5U19 DK61934), the Defense Advance Research Programs Agency (F30602-00-2-0609 Simbiosys), and Stanford Bio-X.

Received for review October 16, 2002. Accepted December 6, 2002.

AC026239A